Accepted Manuscript version of paper accepted on 11 September 2024 for publication in *Railway Engineering Science*, doi: 10.1007/s40534-024-00359-z

# Methods for separating the noise produced by the wheels and track during a train pass-by

David Thompson[1*], Dong Zhao[1], Giacomo Squicciarini[1], Martin Toward[1], Ester Cierco[2], Erwin Jansen[3] and Michael Dittrich[3]

[1]Institute of Sound and Vibration Research, University of Southampton, Southampton SO17 1BJ, United Kingdom
*: Corresponding author, Email: djt@isvr.soton.ac.uk

[2]Ingeniería para el Control del Ruido SL, Berruguete 52 08035 Barcelona, Spain

[3]TNO Acoustics and Sonar, Oude Waalsdorperweg 63, 2597 AK, The Hague, The Netherlands

**Abstract**

Rolling noise is produced by vibration of the wheels and track, induced by their combined surface roughness. It is important to know the relative contributions of the different sources, as this affects noise control strategies as well as acceptance testing of new rolling stock. Three different techniques are described that aim to use pass-by measurements to separate the wheel and track components of rolling noise. One is based on the TWINS model, which is tuned to measured track vibration. The second is based on the advanced transfer path analysis method, which provides an entirely experimental assessment. The third is based on the pass-by analysis method in combination with static vibroacoustic transfer functions which are obtained using a reciprocity method. The development of these methods is described and comparisons between them are presented using the results from three experimental measurement campaigns. These covered a metro train, a regional train and a high-speed train at a range of speeds. The various methods agree reasonably well in terms of overall trends, with moderate agreement in the mid-frequency region, and less consistent results at low and high frequency.

**Keywords**: Rolling Noise, Source Separation, Pass-by Tests.

## 1. Introduction

New mainline trains in Europe must comply with noise limits as defined in the Technical Specification for Interoperability, TSI Noise [1]. These include pass-by tests at constant speed, as well as tests under stationary and starting conditions and noise within the driver's cab. The pass-by tests should normally be carried out on a reference track that meets certain requirements, in particular in terms of its track decay rates and rail roughness levels, as specified in EN ISO 3095:2013 [2]. The purpose of these requirements is to minimise the influence of the track on the measured noise so that the measurement is mainly characteristic of the vehicle noise, allowing quiet or noisy vehicles to be identified. However, it can often be difficult or costly to access or maintain a track that fulfils these TSI track requirements. Moreover, these requirements do not eliminate the influence of the track, which is a source of significant variation between test sites.

The main source of noise during the pass-by test is rolling noise, which is radiated by vibration of both the track and the wheels, excited by their combined surface roughness. A reliable separation of the vehicle and track contributions to rolling noise could be used in future as a basis for a revised test procedure that would avoid the strict requirements on the track properties. In the past, several different methods have been proposed to separate the contributions of vehicle and track to the rolling noise. These include methods based purely on measurements, on calculations, or on a combination of both.

Different levels of separation were proposed in [3], in which level 1 consists of separation of the sound pressure contributions of vehicle and track, level 2 the separation of vehicle and track transfer functions and roughness spectra, and level 3 includes additional dynamic quantities that might be required for non-standard wheels or tracks. The pass-by analysis (PBA) method was then developed, in which the combined wheel/rail roughness is derived from the rail vibration, making use of various model-based correction factors [3]. Methods to determine the track decay rate from the rail acceleration were also developed. These various methods based on PBA have since been published as Technical Report by the European Committee for Standardization (CEN) [4]. A related objective of these separation methods is to allow transposition of noise results from one site to another and from one train to another. This concept was further tested in the Acoutrain project [5, 6].

Theoretical models allow the various components of noise to be quantified. In an early study, Remington [7] found, for a situation with small wheels, that most of the noise was radiated by the track. Thompson [8] used models of the sound radiation together with measured vibration spectra to separate wheel and rail noise, finding that the rail was dominant between 400 and 1000 Hz, and the wheel was dominant at frequencies above 1250 Hz; the wheel design in this case had a larger than

usual diameter. These models have been developed into the TWINS model [9, 10], which has also been used to identify the wheel, rail and sleeper components of noise in terms of one-third octave spectra. It is found that the sleepers are generally dominant at low frequencies, the rails in the mid frequencies and the wheels at high frequencies.

Experimental methods based on microphone arrays have widely been used to separate sources on moving vehicles, especially aerodynamic sources. When they have been used to study rolling noise [11–17], however, they often show that the wheel is the dominant source, whereas analysis based on models such as TWINS [9, 10] shows that the rail can be the dominant source in much of the frequency range. Kitagawa and Thompson [18, 19] showed that the source strength associated with the rail radiation may not be detected correctly due to the inherent assumptions within the beamforming analysis. This analysis relies on a source model, in which the source region is usually represented as a distribution of uncorrelated omnidirectional point sources. It is shown in [20] that, due to source directivity, a typical microphone array would overestimate the contribution of a dipole source (orientated normal to the track) by around 2 dB and for a corresponding longitudinal quadrupole this difference increases to 3 dB. Additional difficulties are encountered for the noise from the rail, which consists of an extended, correlated source [21, 22]. The radiation from the rail occurs in the form of plane waves orientated at a particular angle to the track. Consequently, a microphone array directed normal to the track will not detect a large part of the noise from the rail, with differences of up to 10 dB being found [18]. Some advanced methods have been developed recently to take account of this effect [23, 24], but this is still an area requiring further research.

A ‘reference vehicle method’ was proposed in the METARAIL project, in which measurements of the pass-by noise from a vehicle with a low vibroacoustic transfer function would be used to characterise the track contribution [15]. In practice, however, it is difficult to find such a vehicle, although some vehicles with very small wheels can be used effectively. Although it was suggested to use shielding on the vehicle, this is less suitable as it can interfere with the track sound radiation. In addition, in [15] the use of an ‘equivalent forces’ method [25] was proposed in which pass-by measurements of vibration are combined with a set of vibroacoustic transfer functions that are measured on the track; this corresponds to a form of transfer path analysis.

An extensive field test was carried out in the Roll2Rail project in 2016 [26, 27] to compare several wheel/track separation techniques. These included an advanced transfer path analysis (ATPA) method [28], the PBA method [3], and a method based on the TWINS model [12] tuned to experimental data. A microphone array was also used in an attempt to identify the wheel component, but this was unsuccessful. A wave signature extraction method [24], based on a one-dimensional microphone array located close to the rail, was also tested and could identify the rail component for frequencies up to 2

kHz; for higher frequencies a denser microphone spacing would be required. A multiple input-single output (MISO) method developed previously in the STAIRRS project [29] was also tested.

These field tests in Roll2Rail considered a single train at a single site, which had a low rail pad stiffness and consequently a high track component of noise. The frequency range was limited to 315–5000 Hz. Each of the techniques considered could determine the track contribution with acceptable accuracy, within 1–2 dB [27]. The ATPA method in particular gave promising results, but it was considered relatively costly in relation to the TSI test. For the wheel component, only the TWINS-based method achieved sufficient accuracy, although this could not be checked independently. To use the PBA method for vehicle/track separation, additional transfer functions are required that were not measured.

The objectives of the current work are to develop further the most promising methods for separating the contributions of vehicle and track to rolling noise during a train pass-by and to apply them over a wider range of conditions. Of the methods considered in [26, 27], ATPA, PBA and the TWINS-based methods have been selected for further development and evaluation. The aim is to separate the track from the wheel contributions, and if possible, to extract the separate rail vertical, rail lateral and sleeper components from the track. Ideally, the frequency range should be extended to cover 100-8000 Hz. Three new field test campaigns have been carried out to allow an extension of the validation of the various separation methods. These are for a metro train, a regional train and a high-speed train.

In Section 2 the methods and their enhancements are described. The three field test campaigns are described in Section 3. The results of these measurements, including the comparisons of the separation methods, are presented in Section 4. Conclusions are summarised in Section 5. Some preliminary results were presented in [30].

## 2. Separation methods

### 2.1 TWINS-based method

TWINS [8] consists of a series of engineering models and has been validated against extensive field experiments in the 1990s [9, 31]. For the wheel vibration it is based on modes derived from a finite element model and for the track vibration it uses analytical models. As it predicts the noise radiation from the wheel, rail and sleeper separately, it can be used to identify these components of noise. However, it should be noted that, apart from some checks of intermediate results such as track and wheel vibration, validation of the model has relied on comparing the measured noise spectra with the total predicted noise spectra, as there is no independent reference result available for the source

separation. Consequently, the separation results may be subject to greater uncertainty than the overall noise spectra, especially for the components giving a smaller contribution in a given frequency band.

Making use of the intermediate comparisons of vibration, it has been identified that the parts of the model used to calculate the noise radiation are more reliable than those used for predicting the vibration from the surface roughness [9, 31]. Consequently, the uncertainty in the estimates of the component contributions can be reduced by combining the model with vibration measurements obtained during a train pass-by. To apply TWINS to source separation, therefore, the following steps are applied [26, 27].

First, the input parameters for the track are chosen to give the best possible fit to static measurements of the track mobilities and decay rates. The most important parameters are the stiffness and damping of the rail pads and the ballast. The modal damping ratios of the wheels are measured and used to ensure the finite element model gives good agreement with measured mobilities; no other tuning is applied to the finite element model. The wheel and rail roughness spectra are also measured and used as input to the TWINS predictions; the measured track decay rates are also used in the predictions.

Having established a TWINS model corresponding to the measured situation, the level differences between predicted and measured vibration spectra are determined for the rail (in two directions) and the sleeper. Ideally, these differences should be as small as possible. The spectral estimates of noise from each of these three components are then estimated by adjusting the outputs from the model in accordance with these level differences:

$$L_{p,i,j} = L_{p,i,j}^{\mathrm{TWINS}} + L_{v,i}^{\mathrm{meas}} - L_{v,i}^{\mathrm{TWINS}} \quad (1)$$

where $L_{p,i,j}$ is the sound pressure level from component $i$ in frequency band $j$. Superscript TWINS indicates outputs from the model and superscript ‘meas’ is from the measurement.

Finally, the total predicted noise is determined by adding the various components, including the wheel noise, and the difference between the predicted and measured noise spectra is used to assess the accuracy of the estimates. As it was not possible to measure the wheel vibration the wheel noise is not adjusted in this process, based on the assumption that the differences between measured and predicted track vibration are caused by inadequacies in the track vibration model.

In the current work, several improvements have been made to the TWINS-based separation method compared with the approach used in Roll2Rail [26, 27]. Although the models are referred to as TWINS, an in-house implementation in Matlab is used which allows more flexibility. This mainly includes the same sub-models as the commercial software but with some improvements. It includes a

new implementation of the flexible sleeper model [22]. To include the frequency-dependent dynamic stiffness of the ballast, a continuous foundation of springs and viscous dampers is applied beneath the sleeper [32].

Recently developed models for the sound power radiated by the track have been introduced [33–35]. The sound power radiated by the rail is calculated using two-dimensional (2D) boundary element (BE) models for the rail in proximity to the ground. A weighted average is used of the results for the rail located 50 mm above the ballast surface and the rail attached to the sleeper. For the sleeper radiation, radiation efficiencies are calculated allowing for the interaction between three adjacent sleepers. These are calculated using three-dimensional (3D) BE models, including the effect of the ballast absorption.

The effect of the vehicle on the sound radiation from the rail is also included by using 2D boundary element models [36]. These models are used to determine the sound pressure at the receiver for a unit vibration amplitude of the rail, allowing for the ground geometry and the effect of reflections from the underside of the vehicle. Again, a weighted average is used of the results for the rail 50 mm above the ballast and the rail attached to the sleeper. For the sleeper, no ground reflections are included, but the directivity in the vertical plane is assumed to be omnidirectional in a half space.

Finally, as two of the test sites (see below) were fitted with stiff rail pads, it was found to be necessary to use a discretely supported track model in the calculations for these sites. The average over results calculated for five contact positions within half a sleeper span is used to estimate the noise (and track vibration) during the train passage.

## 2.2 Advanced transfer path analysis method

The ATPA method [28] is based on extensive transfer function measurements of the track, preferably obtained with the vehicle present; these are combined with operational measurements of sound pressure and track vibration.

First the relevant track section is defined. Its length depends on the distance of the microphones from the track; for a distance of 3.5 m, a length of around 7 m is typically used but for a larger microphone distance the track section should be longer. This track section is then divided into subsections or sectors, as shown in Fig. 1 (here there are seven, each with a length of two sleeper bays). For each sector, the vertical and lateral acceleration of both rails and the vertical acceleration of the sleeper are

treated as separate subsystems. The corresponding measurement locations are located in the centre of each subsystem and are indicated schematically in Fig. 1. For the arrangement shown, this gives a total of 5×7=35 subsystems.

Transfer functions are measured between each pair of subsystems. These transfer functions take the form of transmissibilities (ratios of acceleration at the different points, $a/a$) when each of the subsystems in turn is excited by a hammer; they are referred to in the ATPA method as 'global transfer functions (GTF)' [28]. The hammer excitation is applied at randomly distributed positions within the subsystem. In addition, the sound pressure is measured at the receiver points and expressed as transfer functions of pressure divided by acceleration, $p/a$.

A matrix operation is then used to obtain the 'direct transfer functions (DTF)' $T^D_{k\to M}$ which express the sound pressure at a receiver point $M$ due to vibration in one subsystem $k$ when the response of all other subsystems is blocked [28]. By combining these direct transfer functions with the acceleration spectra measured during the train passage $a_k$, the total noise at a receiver location $M$ (in a given frequency band) can be decomposed into the components associated with each subsystem

$$p_M = \sum_{k=1}^{N} a_k T^D_{k\to M} \tag{2}$$

where $a_k T^D_{k\to M}$ directly gives the component associated with subsystem $k$.

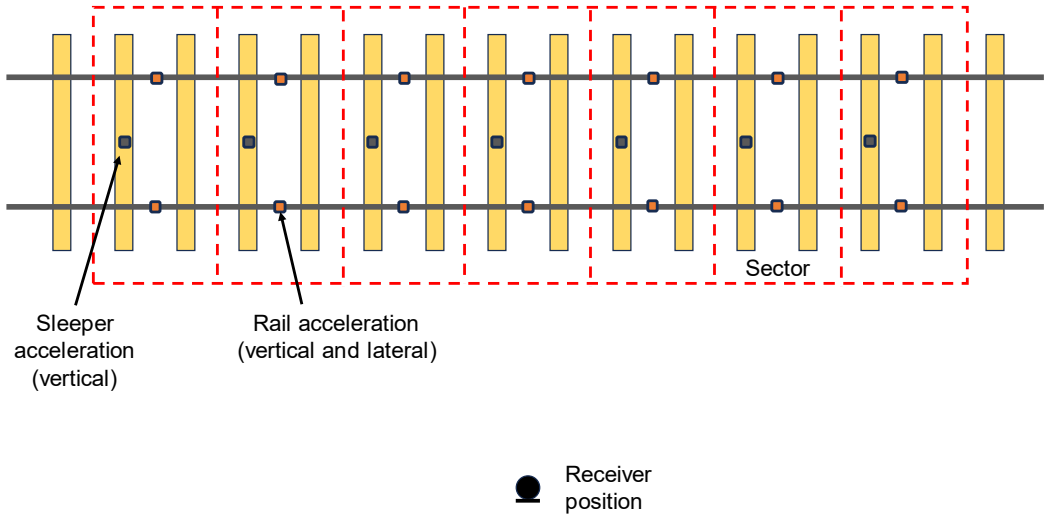


Figure 1. Experimental arrangement used for ATPA method.

Although it is preferable to measure these transfer functions with the vehicle present on the track, this is not always possible and, moreover, if it can be avoided it can reduce the costs of the tests. This was the case for two of the three measurement sites. An allowance for the effect of the vehicle can be made using either boundary element calculations (as used for the TWINS predictions [36]) or using results from previous measurement campaigns in which measurements have been performed in both configurations from which the difference can be extracted.

Commonly, the signal-to-noise ratio at 7.5 m from the track centre is insufficient when using hammer excitation. A microphone position at 3.5 m from the track has therefore been used. 2D BEM calculations (similar to [36]) were used to confirm that there are no major differences in the distribution of the various components at these two positions.

In the set-up shown in Fig. 1 there are 35 accelerometers attached to the track. To reduce the cost of the method, it would be advantageous to use a smaller number of transducers, especially during the pass-by measurements. In [26] it was shown that it is possible to use the five accelerometers of a single-track sector and to estimate the vibration at others by applying a suitable time delay. This relies on the rail roughness (and track dynamics) not varying significantly between track sectors. Applying this to the test case in [26] gave a maximum overall difference of 0.3 dB in the track noise estimation. This reduction in instrumentation can be advantageous to minimise the time required for the test schedule. However, if the whole set of accelerometers is already installed for the static tests, it may be left in place for the pass-by tests and there is no need for the reduction.

In the current tests, a reduced number of accelerometers (three sectors instead of seven) was installed on the track for the pass-by measurements at the high-speed site, as there was insufficient time available to install the full instrumentation. Therefore, the results for other sectors were reconstructed by applying the corresponding delays to the measured signals.

### 2.3 Pass-by analysis methods

In the original PBA method [3, 4], measurements of rail acceleration and sound pressure at the trackside are used to determine the total equivalent roughness and a total roughness-to-noise transfer function. Track decay rates are also extracted from these signals and used as part of the procedure. By comparing the roughness-to-noise transfer functions obtained at different speeds, the rolling noise can be isolated from the contribution of other sources.

In the current work, this PBA method was combined with static transfer functions of the wheel and the track. The static transfer functions are used to achieve a separation of the rolling noise into the contributions from different components.

Static transfer functions from applied force to sound pressure can be measured using either direct or reciprocal methods. In the direct method, the track or wheel is excited by an instrumented impact hammer in different directions and the transfer function is measured from the force $F_1$ to the pressure $p_2$ at the wayside microphone position. In the reciprocal method [37], a sound source of known volume velocity $q_2$ is placed at the microphone position and the resulting vibration velocity $v_1$ of the track or wheel is measured. These two transfer functions are equivalent, as follows:

$$\left(\frac{v_1}{q_2}\right)_{\text{reciprocal}} = \left(\frac{p_2}{F_1}\right)_{\text{direct}} \tag{3}$$

The reciprocal method is used here as it generally gave better a signal-to-noise ratio.

The transfer function has the form $p/F$, where $p$ is pressure at the receiver and $F$ is a force. They are then converted to the form $p/r$, where $r$ is the roughness spectrum, using

$$\left(\frac{p}{r}\right)_i = \left(\frac{p}{F}\right)_i \times \frac{F_i}{r} \tag{4}$$

where the subscript *i* indicates the force direction. For the vertical direction the force per unit roughness $F/r$ can be obtained from a sum of receptances [22]:

$$\frac{F}{r} = \frac{1}{\alpha_{\mathrm{w}} + \alpha_{\mathrm{r}} + \alpha_{\mathrm{c}}} \tag{5}$$

in which $\alpha_{\mathrm{w}}$ is the wheel receptance, $\alpha_{\mathrm{r}}$ is the rail receptance, and $\alpha_{\mathrm{c}}$ is the receptance of the contact spring. The receptances $\alpha_{\mathrm{w}}$ and $\alpha_{\mathrm{r}}$ in Eq. (5) may be either measured or predicted using the TWINS model. To obtain the lateral force, use is made of a matrix version of Eq. (5) [22], also contained within TWINS.

The vertical and lateral interaction forces are applied to the corresponding $p/F$ transfer functions. A weakness of this approach is that a vertical force applied to the rail also excites the sleeper. To determine the sleeper component separately, an estimate of the force acting on the sleeper is derived from the ratio of the responses of the sleeper and the rail to a force acting on the rail. Both wheel and track radiation can be estimated if their $p/F$ transfer functions have been measured; however, for the wheel it is found to be important that the damping is at a similar level in the transfer function measurement to that present in a rolling wheel [38]; the use of undamped transfer functions would lead to an overestimate of the wheel contribution.

Ideally, the static transfer functions of the wheel and track should be measured separately by lifting the wheel clear of the track. However, this was not possible at any of the test sites. Therefore, static transfer function measurements of the wheel could only be performed with the wheel in contact with the rail. This means that the rail also radiates sound when the wheel is excited (and vice versa) which will affect the vibro-acoustic transfer functions to some extent. On the rail, the excitation position (the location of the accelerometer in the reciprocal method) was close to the contact point with the wheel (within about 10 cm). On the wheel, the excitation position was at about 45° from the contact point.

All individual transfer functions $p/r$ for each component and direction are summed to form a combined transfer function. By comparing the individual transfer functions with the combined one, 'distribution functions' are derived that indicate the relative importance of each source. Finally, these distribution functions are applied as weighting factors on the measured pass-by spectrum of rolling noise at each speed.

## 3. Field tests

Field tests have been carried out for three different trains; these are a metro train, a regional train and a high-speed train. Each was measured at its own corresponding test site. Characterisation of the test sites and the trains is described in this section. In each case the wheel was modelled using axisymmetric finite elements. The wheel mobilities were measured in a depot with the wheel lifted clear of the rail and the measured modal damping ratios were used in the predictions. The rail mobility was measured in both vertical and lateral directions and used to tune the values of rail pad stiffness and damping. Track decay rates (TDR) were also measured for vertical and lateral vibration. The wheel roughness was measured on all wheels of the test bogies and the rail roughness of the test sites was measured on both rails. Further details of the measurements are given in [38].

### 3.1 Site 1: metro train

The measurement site used for the metro train was on a metre gauge line in Spain. The rail was of type RN45, mounted on concrete sleepers. The train was a four-car electric multiple unit (EMU), with a maximum speed of 90 km/h. The wheels have diameter 850 mm and are fitted with ring dampers; the train is braked by axle-mounted disc brakes. The measurements focused on two adjacent trailer bogies in the centre of the train, for which the noise is dominated by rolling noise. The length of this section (two half-vehicles) is 17 m. The predicted wheel mobilities in the radial direction are shown in Fig. 2a and compared with the measurements, showing very good agreement apart from a small shift

in natural frequencies. The measured results appear to be affected by a limited signal-to-noise ratio at low frequencies.

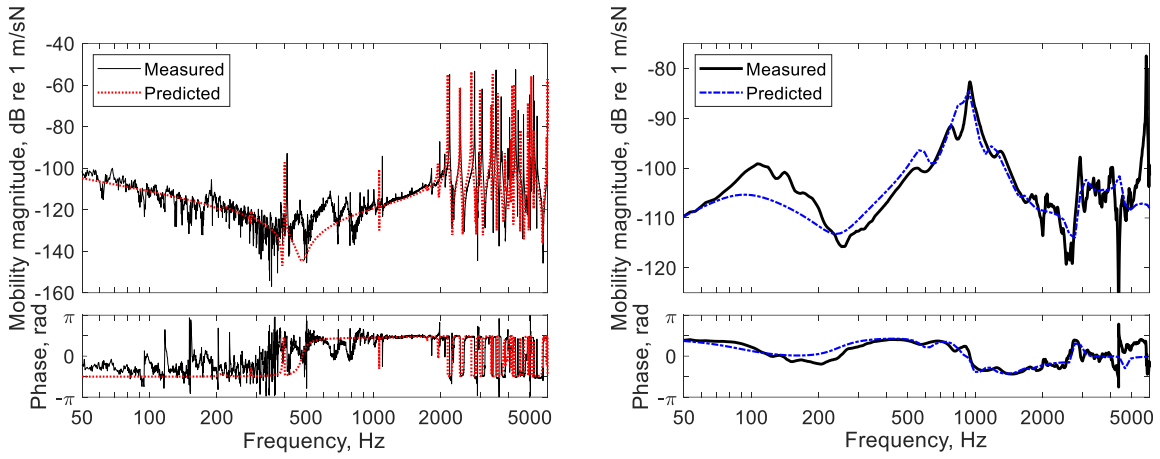


(a) (b)

Figure 2. Measured and predicted mobilities for metro train site: **a** radial wheel mobility; **b** vertical track mobility at mid-span.

The vertical track mobility is shown in Fig. 2b. This was obtained at the mid-span position between two sleepers. The strong peak at about 1 kHz corresponds to the pinned-pinned resonance. Due to the stiff rail pads used at this site, there are strong differences between the mobility at mid-span and above a sleeper (not shown). Therefore, the corresponding predicted result shown in Fig. 2b is based on a discretely supported track model with the rail represented as a Timoshenko beam and the sleepers also represented by beams. The parameters used in the track model are listed in Table 1. Other smaller peaks in the region 500–1500 Hz correspond to resonances of the sleepers. The peak at 5 kHz corresponds to a foot-flapping mode of the rail [22], not predicted using the Timoshenko beam model.

Table 1. Parameters used for the tracks.

| Parameter | | Metro site | Regional site | High-speed site |
|---|---|---|---|---|
| Rail | Vertical bending stiffness ($MNm^2$) | 3.28 | 6.42 | 6.42 |
| | Lateral bending stiffness ($MNm^2$) | 0.60 | 1.07 | 1.07 |
| | Mass per unit length (kg/m) | 45 | 60 | 60 |
| | Damping loss factor | 0.02 | 0.02 | 0.02 |
| | Shear coefficient | 0.4 | 0.4 | 0.4 |
| | Cross mobility factor (dB) | -7 | -7 | -7 |
| Pad | Vertical stiffness per pad (MN/m) | 1000 | 1500 | 220 |
| | Lateral stiffness per pad (MN/m) | 75 | 75 | 25 |
| | Damping loss factor | 0.2 | 0.2 | 0.2 |
| Sleeper | Mass (half sleeper) (kg) | 100 | 150 | 150 |
| | Young's modulus (GPa) | 41.3 | 41.3 | 41.3 |
| | Poisson's ratio | 0.15 | 0.15 | 0.15 |
| | Damping loss factor | 0.02 | 0.02 | 0.02 |
| | Spacing (m) | 0.6 | 0.6 | 0.6 |
| | Length (half sleeper) (m) | 0.95 | 1.3 | 1.3 |
| | Height (rail seat) (m) | 0.227 | 0.22 | 0.22 |
| | Height (centre) (m) | 0.227 | 0.18 | 0.18 |
| | Width (real seat, top) (m) | 0.263 | 0.26 | 0.26 |
| | Width (rail seat, bottom) (m) | 0.263 | 0.30 | 0.30 |
| | Width (centre, top) (m) | 0.263 | 0.20 | 0.20 |
| | Width (centre, bottom) (m) | 0.263 | 0.22 | 0.22 |
| Ballast | Vertical stiffness per sleeper end (MN/m) | 60 | 60 | 160 |
| | Vertical damping coefficient per sleeper end (kNs/m) | 95 | 95 | 166 |
| | Lateral stiffness per sleeper end (MN/m) | 35 | 35 | 35 |
| | Lateral damping loss factor | 2.0 | 2.0 | 2.0 |

The TDRs are shown in Fig. 3; the limits from ISO 3095:2013 [2] are shown for comparison. Generally good agreement is obtained between the predictions and the measurements. The vertical TDR remains high until 1.6 kHz, which is consistent with a high value of rail pad dynamic stiffness. The lateral TDR drops at around 300 Hz and corresponds to a much lower value of rail pad stiffness. From these measurements of mobility and TDR, the rail pad stiffness was derived as 1000 MN/m for the vertical direction and 75 MN/m for the lateral direction; the damping loss factor was set to 0.2.

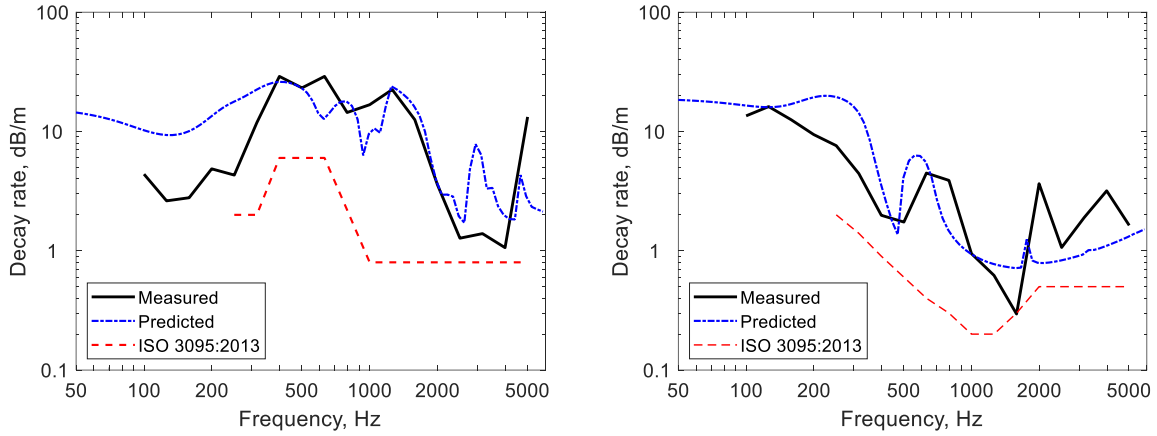


Figure 3. Measured and predicted track decay rates for metro train site: **a** vertical; **b** lateral.

Train pass-bys were measured with a test train during a full nighttime track possession, allowing the train to run in both directions. Three train pass-bys were measured at each of four speeds, 40, 60, 80 and 90 km/h. Data from all test runs were used in the TWINS analysis. However, the ATPA analysis is only presented for the three lower speeds due to the presence of many spikes in the pass-by acceleration data at the higher speeds. The PBA method was not available at this site.

### 3.2 Site 2: regional train

The regional train was an 8 car EMU with a maximum speed of 200 km/h and a total length of 165 m. It has four conventional motor bogies with a 2.4 m wheelbase, and six trailer (Jacobs) bogies with a wheelbase of 2.7 m. It has wheel-mounted disc brakes as well as electric braking. The Jacobs bogies have wheels of diameter 850 mm, whereas the motor bogies have larger wheels of diameter 920 mm. The measurements focused on a section of the train consisting of two half-vehicles which shared a single Jacobs bogie. The length of this test section is 18.5 m. The predicted and measured wheel mobilities in the radial direction for the test bogie are shown in Fig. 4a, showing generally good agreement.

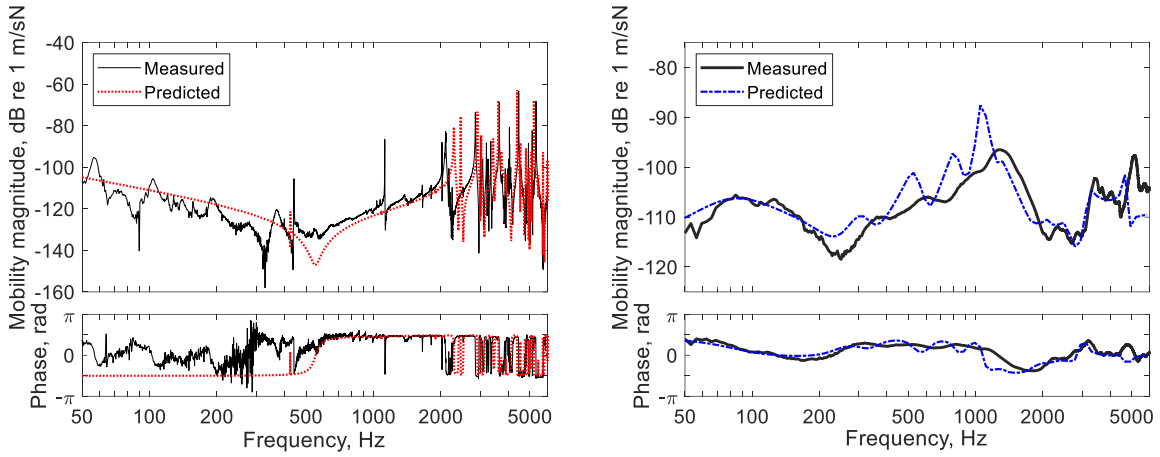


(a) (b)

Figure 4. Measured and predicted mobilities for regional train site: **a** radial wheel mobility; **b** vertical track mobility at mid-span.

The measurements were carried out on a test track that is routinely used for TSI-compliance testing. The track is fitted with 60E1 rail, stiff rail pads and rail dampers. A large number of train pass-bys were measured at speeds ranging from 40 to 200 km/h.

The measured and predicted vertical track mobility is shown in Fig. 4b for the mid-span position between two sleepers. The parameters used in the track model are listed in Table 1. The strong peak in the predictions at about 1 kHz again corresponds to the pinned-pinned resonance; as for the metro train site, due to the stiff rail pads at this site it is necessary to use a discretely supported track model. As the test site was fitted with rail dampers, the measured mobility is lower than the predicted one in the mid-frequency region; the model does not include the rail dampers. The corresponding TDRs are shown in Fig. 5. The measured results are higher than the predictions due to the installation of rail dampers, especially for the lateral direction. The rail pad stiffness was set to 1500 MN/m in the vertical direction and 75 MN/m in the lateral direction, with a loss factor of 0.2.

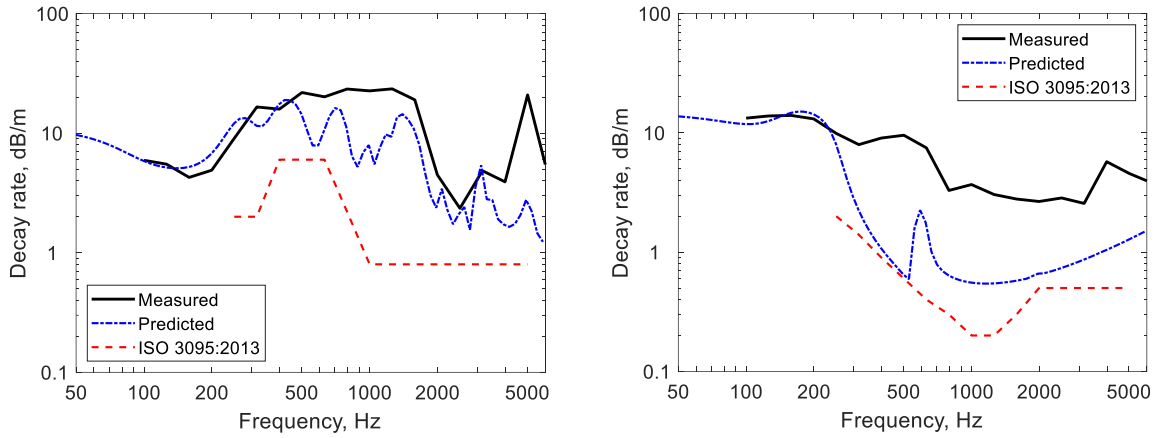


Figure 5. Measured and predicted track decay rates for regional train site: **a** vertical; **b** lateral

3.3 Site 3: high-speed train

The high-speed train had a power car with conventional motor bogies at each end of the train and 12 articulated trailer vehicles with single pairs of wheels at each connection. The trailer wheels have a diameter of 920 mm and are fitted with wheel-mounted disc brakes. The measurement focused on a test section consisting of three vehicle-lengths (overall length 39.6 m) containing three single wheels (on each side of the train). The predicted and measured wheel mobilities for the radial direction are shown in Fig. 6a, showing good agreement.

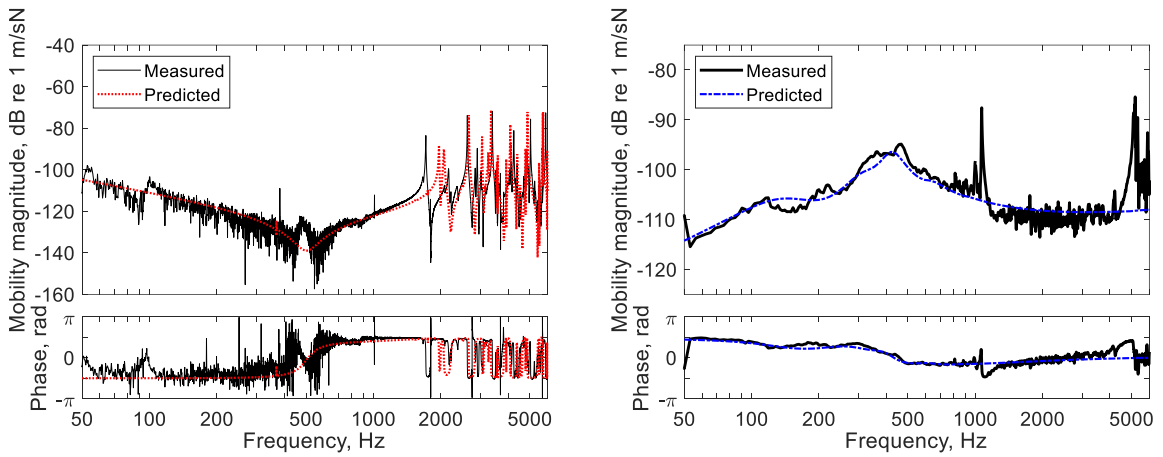


Figure 6. Measured and predicted mobilities for high-speed site: **a** radial wheel mobility; **b** vertical track mobility at mid-span.

The high-speed test campaign was carried out on a high-speed line in Spain. One track was instrumented and the train ran in both directions past the test site during an overnight line closure. The

test site is fitted with 60E1 rails, moderately soft rail pads and concrete sleepers. The maximum speed at this site was 280 km/h.

The vertical track mobilities at this site are shown in Fig. 6b. These were again obtained at the mid-span position. However, since the rail pad is much softer than at the other sites, the mobilities at mid-span and above a sleeper (not shown) are very similar and the conventional continuously supported Timoshenko beam track model is used. For the vertical direction, the agreement with the predictions is very good, apart from the sharp peak at the pinned-pinned frequency (1 kHz) and the peak at 5 kHz (foot-flapping mode) which are not predicted using this continuously supported Timoshenko beam model. The parameters used in the track model are listed in Table 1.

The corresponding TDRs are shown in Fig. 7. They are much lower than for the other sites due to the softer rail pads. The predictions agree well with the measured results for both lateral and vertical directions. For the vertical direction the TDR drops from its low frequency plateau at around 400-500 Hz. There is also a clear peak in the vertical mobility at around this frequency, from which the vertical dynamic pad stiffness of 220 MN/m is identified. The lateral rail pad stiffness was identified as only 25 MN/m; again, a loss factor of 0.2 was used. Unlike the other tracks described in the previous sections, at this site both vertical and lateral TDRs have very low values at high frequencies, with a minimum of around 0.2 dB/m.

The static transfer functions required with the PBA method were measured on a train of the same type on a remote siding of the depot. The transfer functions required for the ATPA method were measured at the test site without the train present for a limited number of sectors as discussed in Section 2.2.

A total of 12 train pass-bys were measured, at speeds ranging from 80 to 280 km/h. Due to interference observed in some of the acceleration signals, not all the vibration signals could be used and no usable results were obtained at 200 km/h.

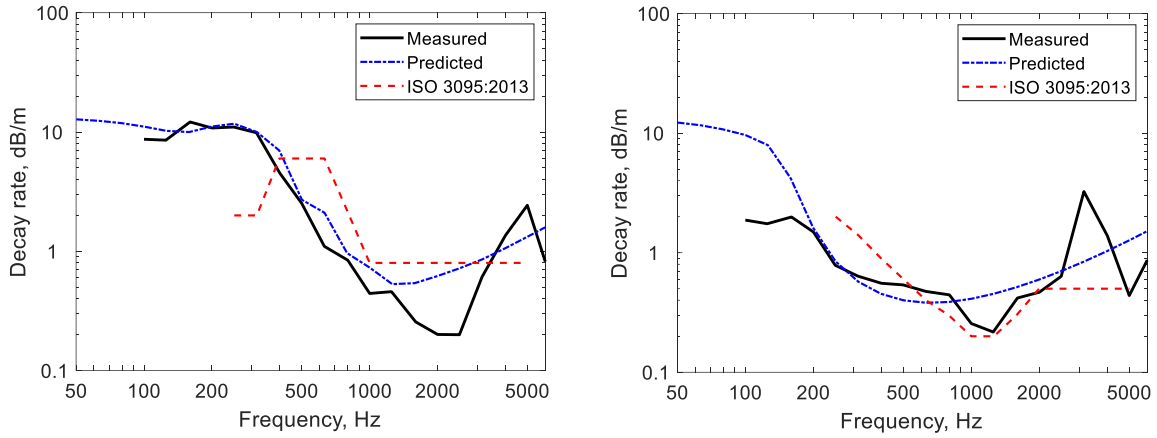


(a) (b)

Figure 7. Measured and predicted track decay rates for high-speed site: **a** vertical; **b** lateral

## 4. Results

For each test site, the results of applying the separation methods are presented in detail for one example speed; results at other speeds were found to be generally similar. All results are presented as A-weighted sound pressure level in one-third octave bands, obtained as the average over the length of the test section of the train. For confidentiality reasons, the results have been normalised so that the average measured A-weighted noise level is equal to 75 dB at 80 km/h. The same normalisation factor has then been applied to all results (measured and predicted) from a given campaign to preserve information on the speed dependence. The ATPA results are based on a microphone at 3.5 m from the track centre, whereas the other methods are based on the standard microphone position at 7.5 m; however, the normalisation has the effect of making the results directly equivalent as the sound pressure level at 80 km/h is still equal to 75 dB (even though the measured results at 3.5 m were higher). Note that, as no operational vibration measurements could be made on the wheels, the wheel noise estimates from the ATPA method are obtained by ‘subtraction’, i.e. taking the energy difference between the measured noise and the track noise estimate.

### 4.1 Site 1: metro train

For the metro train campaign, only the TWINS-based and ATPA methods are available. At this site the ATPA transfer functions have been determined with the train present. Due to limitations of the instrumentation, the results for the ATPA method are limited to a maximum frequency band of 5 kHz at this site. In Fig. 8, the results for the overall track and wheel contributions from these two methods are compared for an example speed of 60 km/h. The TWINS and ATPA methods give similar spectral distributions for the wheel and track, especially for the track contribution.

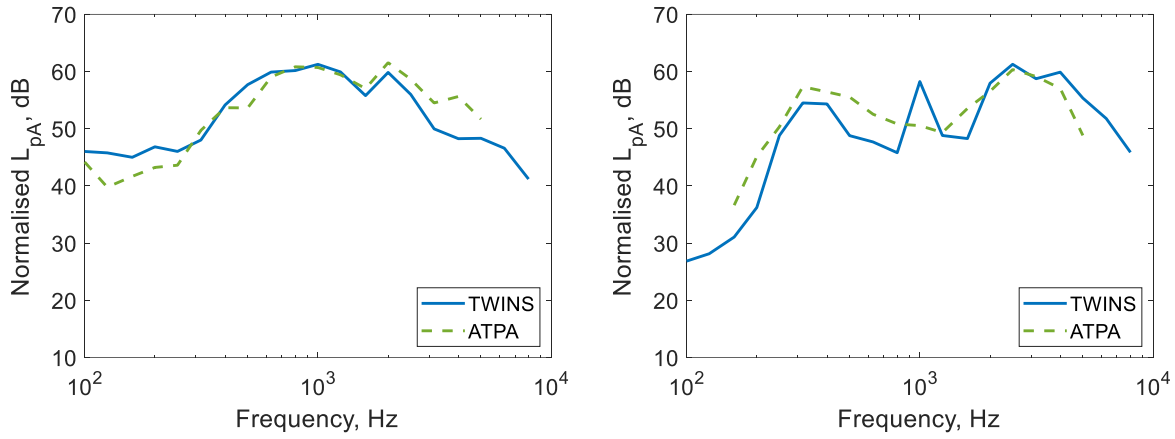


Figure 8. Comparison of the separation results for the metro train at 60 km/h in terms of normalised A-weighted sound pressure level ($L_{pA}$) in one-third octave bands: **a** track component; **b** wheel component.

Figures 9 and 10 compare the separate track contributions. For the rail vertical component in Fig. 9a, the TWINS predictions, based on the measured vibration, are much lower than the results from ATPA, especially at low frequency. Conversely, the sleeper component shown in Fig. 9b shows the opposite trend below 1 kHz, with TWINS giving higher predictions than ATPA. The ATPA results for these two components are quite similar to each other and may be influenced by the strong coupling between the rail and sleeper at frequencies up to more than 1 kHz, as evidenced in the high TDR in Fig. 3a. However, combining these two components (rail vertical plus sleeper), the comparison in Fig. 10a shows much better agreement between the two methods, apart from the region above 3 kHz where the ATPA estimates are higher than those from TWINS. The rail lateral component in Fig. 10b shows very good agreement across the whole frequency range.

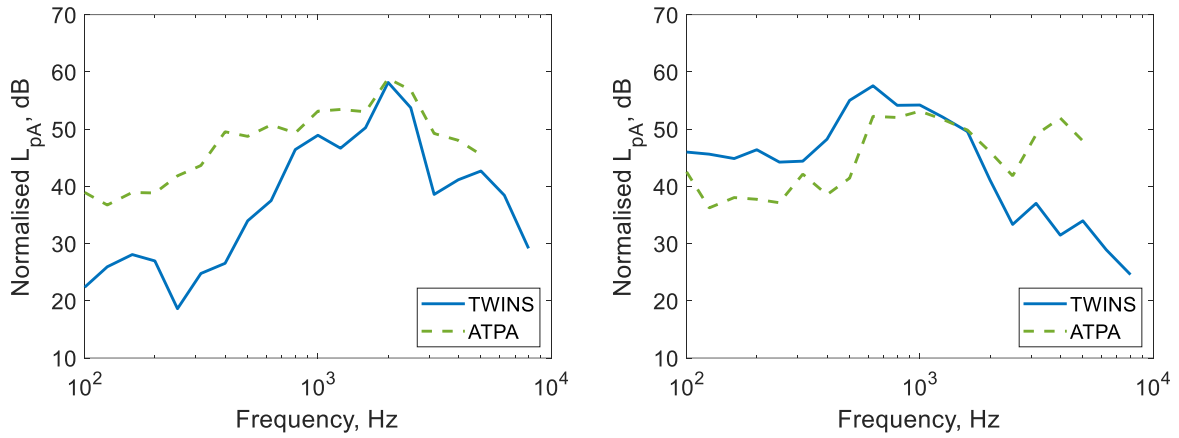


Figure 9. Comparison of the separation results for the metro train at 60 km/h in terms of normalised A-weighted sound pressure level ($L_{pA}$) in one-third octave bands: **a** rail vertical component; **b** sleeper component.

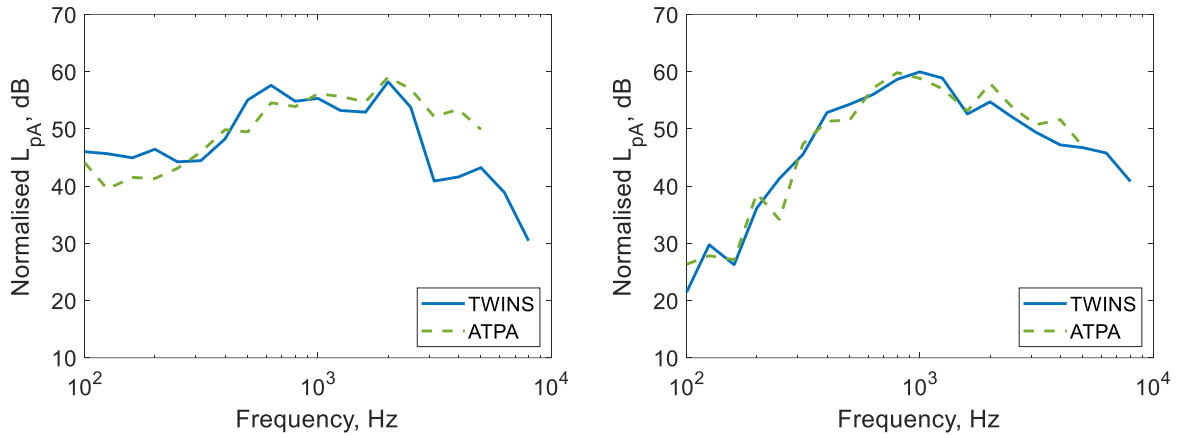


Figure 10. Comparison of the separation results for the metro train at 60 km/h in terms of normalised A-weighted sound pressure level ($L_{pA}$) in one-third octave bands: **a** rail vertical and sleeper component; **b** rail lateral component.

To show the level of consistency of the results for different speeds, Fig. 11a shows the level difference between the total predicted noise spectrum from the TWINS method and the measured spectrum for all four speeds. Also shown in grey is a target accuracy, which was set to ±3 dB between 315 Hz and 5 kHz, which is most important for the overall level, and ±6 dB outside this frequency range. The results all lie within this range apart from an outlier at 40 km/h where a peak appeared in the measured noise at 200 Hz, probably due to another source apart from rolling noise. Results are not shown for the ATPA method in this figure as the total noise is identically equal to the measurement. Fig. 11b shows the level difference between the total predicted A-weighted noise and the

measurement for all four speeds. In this case the target is an accuracy better than ±2 dB, which is achieved in each case.

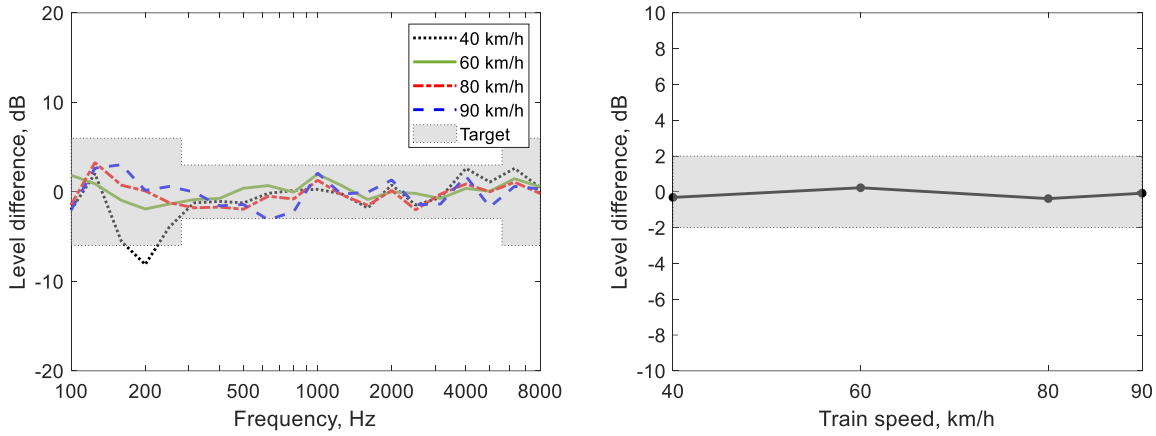


(a) (b)

Figure 11. Level difference between the TWINS prediction and the measurement for the metro train at different speeds: **a** 1/3 octave band spectra; **b** overall A-weighted level.

### 4.2 Site 2: regional train

At this site the ATPA transfer functions have been determined without the train present from frequencies below 500 Hz and with the train for 500 Hz and above. For the PBA method, the track transfer functions measured without the train present were used.

Figure 12 compares the overall track and wheel contributions from the three methods for an example speed of 80 km/h. The separation results for the regional train show larger spectral differences between the different methods than for the metro train. For the track contributions in Fig. 12a there is good agreement in the mid-frequency region; the TWINS-based method gives higher results at low frequency, whereas the ATPA method gives higher results at high frequency (as at site 1 and as also found in [27]). There are larger differences for the wheel component in Fig. 12b, although there is good agreement between TWINS and PBA above 2.5 kHz. Compared with the other methods, ATPA overestimates wheel contribution in the mid frequency region and underestimates it at high frequency. However, it should be recalled that this estimate is based on ‘subtraction’ and so these differences are a consequence of smaller differences in the track noise estimate.

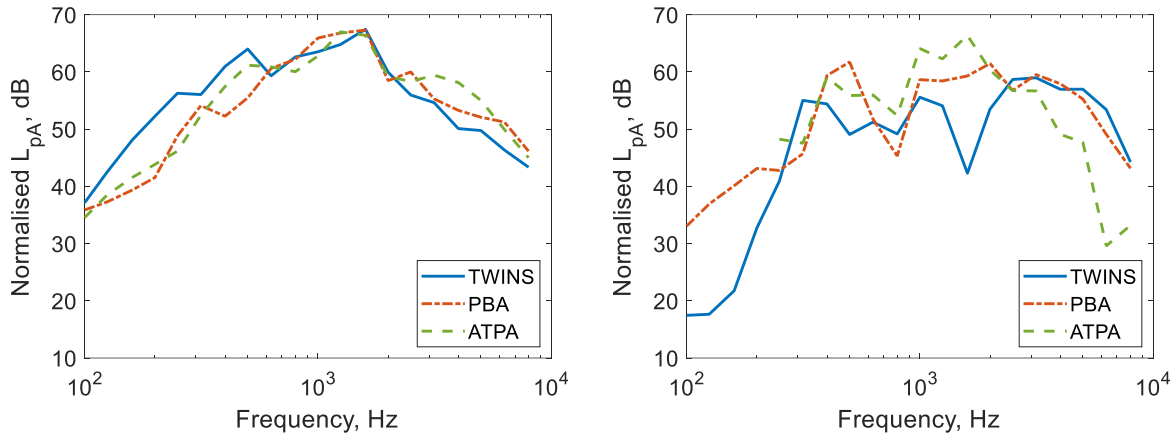


(a) (b)

Figure 12. Comparison of the separation results for the regional train at 80 km/h in terms of normalised A-weighted sound pressure level ($L_{pA}$) in one-third octave bands: **a** track component; **b** wheel component.

Considering the separate track contributions, the ATPA method (and also PBA) gave a higher rail vertical component and a lower sleeper component than the TWINS predictions at low frequency, as found for the metro site (see Fig. 9). Those results not shown here, but the combination of the rail vertical and sleeper components is shown in Fig. 13a; this shows reasonable agreement between the three methods, especially in the region between 315 and 2500 Hz. The rail lateral component in Fig. 13b also shows generally good agreement, although the PBA method gives lower estimates than the other methods at high frequency.

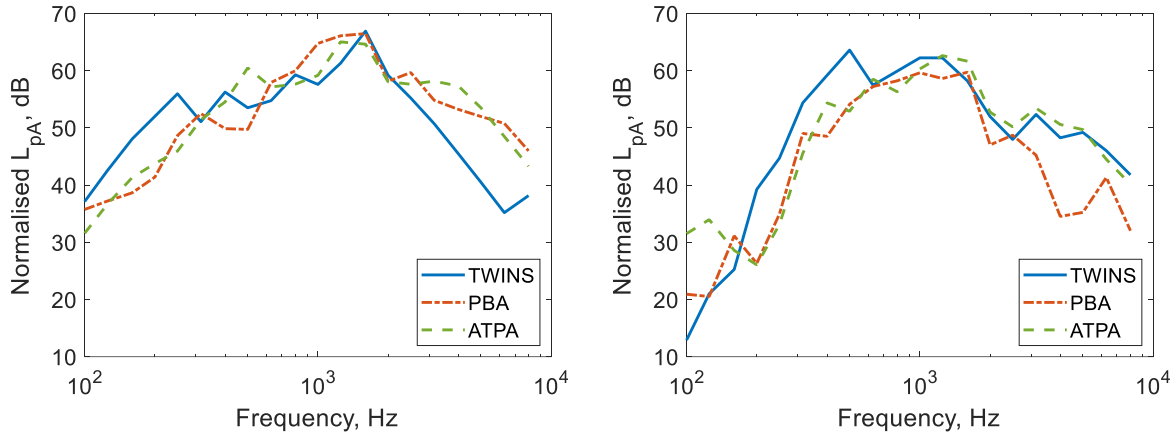


(a) (b)

Figure 13. Comparison of the separation results for the regional train at 80 km/h in terms of normalised A-weighted sound pressure level ($L_{pA}$) in one-third octave bands: **a** rail vertical and sleeper component; **b** rail lateral component.

Figure 14a shows the level difference between the total predicted noise spectrum from the TWINS-based method and the measured one for the lowest five speeds. Also shown in grey is the target accuracy, as discussed above; most results fall within this range. The results at higher speeds (not shown here) contain much larger differences at frequencies below about 1 kHz, which are believed to be caused by the presence of other sources such as aerodynamic noise. Figure 14b shows the level difference between the total predicted A-weighted noise from the TWINS-based method and the measurements for all speeds. For the results for speeds above 120 km/h, the apparent contamination by other sources noted above does not appear to have affected the overall A-weighted level significantly. These results all agree with the measurements better than the target, which is ±2 dB.

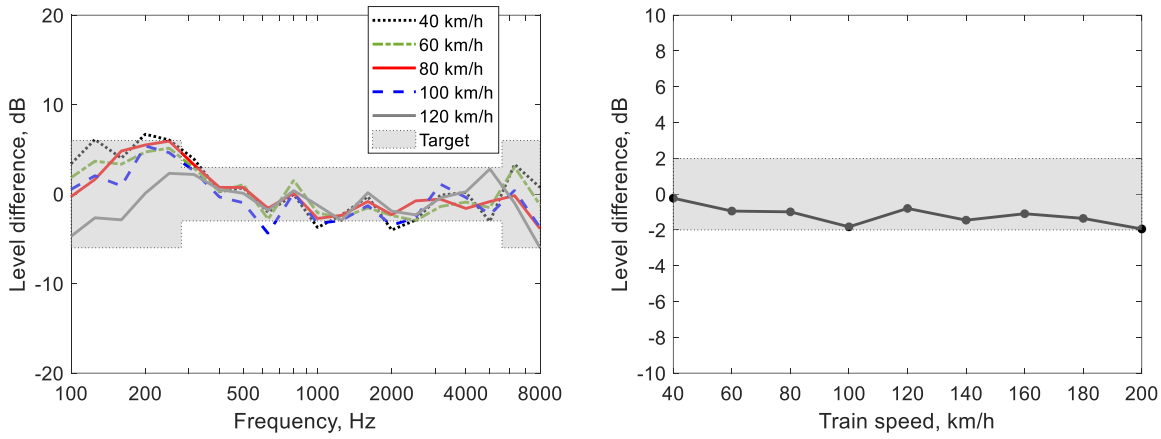


(a) (b)

Figure 14. Level difference between the TWINS prediction and the measurement for the regional train at different speeds: **a** 1/3 octave band spectra; **b** overall A-weighted level.

### 4.3 Site 3: high-speed train

Figure 15 compares the overall track and wheel contributions for an example speed of 80 km/h for the high-speed site. Compared with the other sites, the track noise spectrum in Fig. 15a has higher levels around 500 Hz and above 2 kHz due to the softer rail pads and lower TDR. There is good agreement between the methods for the track contribution in the low and mid-frequency regions. The TWINS-based method and ATPA method also give similar results at high frequency, whereas the PBA results are lower. However, as the transfer functions required by the PBA method were measured in a depot rather than at the test site, this site may have different track properties. Apart from this high frequency region, there are larger differences between the methods for the wheel component in Fig. 15b, although the agreement is slightly better than for the regional train in Fig. 12b. The ATPA results for the wheel are only shown between 250 and 4 kHz as they were considered to be unreliable outside this range.

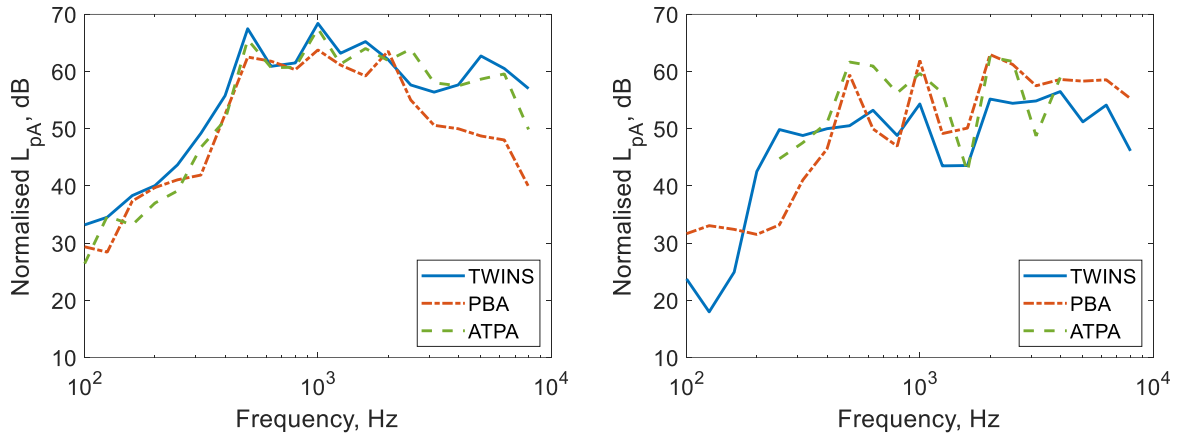


Figure 15. Comparison of the separation results for the high-speed train at 80 km/h in terms of normalised A-weighted sound pressure level ($L_{pA}$) in one-third octave bands: **a** track component; **b** wheel component.

Figure 16 compares the separate track contributions. Although not shown here, the TWINS predictions were again found to give a lower rail vertical component and a higher sleeper component at low frequency than ATPA or PBA. However, due to the softer rail pads at this site the sleeper component is much lower than the rail component for frequencies above 500 Hz (from all methods). Once more, combining the rail vertical and sleeper components, the comparison in Fig. 16a shows good agreement between the three methods, apart from the region above 3 kHz where the ATPA estimates are higher than those from the other methods. The rail lateral component in Fig. 16b shows reasonable agreement, although the PBA method gives much lower estimates at high frequency.

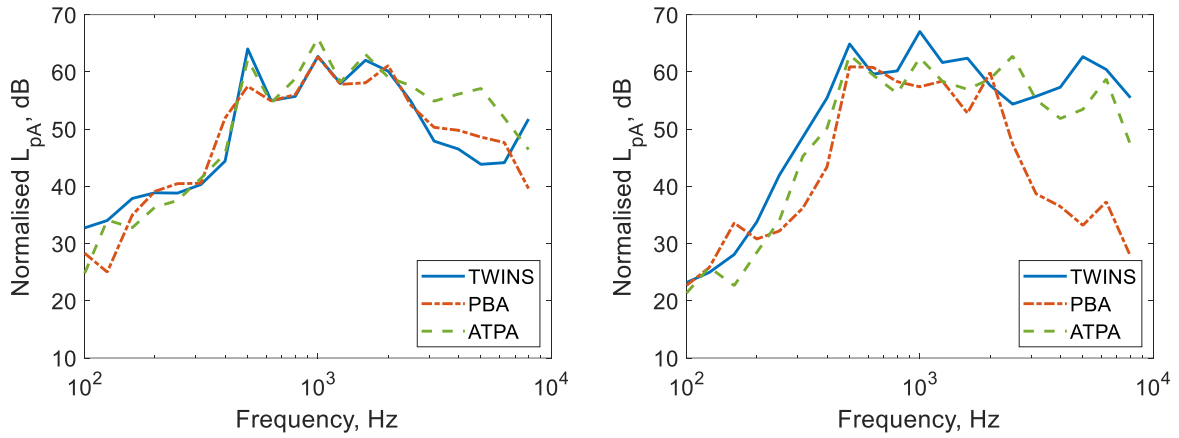


Figure 16. Comparison of the separation results for the high-speed train at 80 km/h in terms of normalised A-weighted sound pressure level ($L_{pA}$) in one-third octave bands: **a** rail vertical and sleeper component; **b** rail lateral component.

Figure 17a shows the level difference between the total predicted noise spectrum from the TWINS-based method and the measured one for the lowest three speeds. Also shown in grey is the target accuracy as discussed above. The results mostly fall within this range, apart from the overprediction at 250/315 Hz, and an underprediction at low frequencies at 120 and 160 km/h.

When the higher speeds are included (not shown here), there are much larger differences at frequencies below about 1.25 kHz. It is believed that this is caused by the presence of other sources such as aerodynamic noise.

Figure 17b shows the level difference between the total predicted A-weighted noise and the measurement for all speeds. For the results for speeds above 160 km/h, the apparent contamination by other sources, noted above, does not appear to have affected the overall A-weighted level significantly. The results all fall within the target range of ±2 dB apart from the highest speed, 280 km/h.

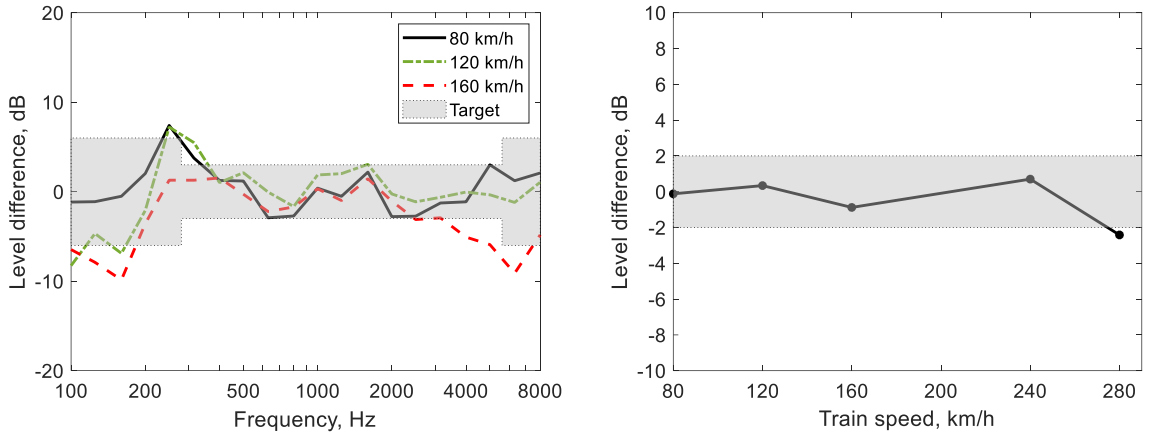


Figure 17. Level difference between the TWINS prediction and the measurement for the high-speed train at different speeds: **a** 1/3 octave band spectra; **b** overall A-weighted level.

### 4.4 Discussion

Considering the results for the total track noise in Figs. 8a, 12a, and 15a, deviations between the results of the three methods are mostly within a range ±3 dB in the frequency region 315–2000 Hz, which is where the track component is particularly important. Less consistent results are obtained at low and high frequency, but the track component is estimated more consistently than the wheel.

The individual track components, especially the rail vertical and sleeper components, are estimated less consistently than the total. Compared with TWINS, both PBA and ATPA overpredict the rail vertical component and underpredict the sleeper component at low frequencies. This seems to be a consequence of strong coupling between these two components. If the two components are combined, more consistent agreement is obtained.

Larger variations between the methods are found for the wheel component of noise (Figs. 8b, 12b, and 15b). The ATPA estimates of wheel noise rely on subtraction of the track noise from the measured total, which can introduce discrepancies when the wheel noise is much lower than the track noise, or when other sources are present. Meanwhile, the PBA estimates are affected by the fact that the transfer functions were measured with the wheel in contact with the track.

The spectral results obtained from the TWINS-based method generally fall within the target range of ±3 dB in the frequency region 315–5000 Hz and ±6 dB outside this region, at least when higher speed runs are omitted (Figs. 11a, 14a, and 17a). The overall A-weighted level is also consistently within the target range ±2 dB (Figs. 11b, 14b, and 17b).

## 5. Conclusions

Three separation methods have been assessed: the first is principally model-based (updated TWINS model, combined with measured track vibration), the second is purely experimental (ATPA) and the third is a hybrid approach (based on PBA combined with static transfer functions). These have been applied to the results of three measurement campaigns.

The analysis focussed on regions of the trains where rolling noise was expected to be dominant. Nevertheless, results at higher speeds are affected to some extent by other sources that are present, so the analysis focuses on lower speeds where rolling noise is dominant.

Moderate agreement is found between the three methods in the mid-frequency region, with less consistent results at low and high frequency. The track component is estimated more consistently than the wheel. The individual track components, rail vertical, rail lateral and sleeper, are estimated less consistently than the total but if the rail vertical and sleeper components are combined, this improves the agreement. As there is no reference result, and each method has limitations, it is not possible to give a definite conclusion about which result is 'correct'. The differences between the various methods are indicative of the inherent difficulties of separating the different source components even using state-of-the-art tools. Nevertheless, it is expected that the TWINS results, based on measured vibration and established radiation models, should be close to the correct result.

In all three methods, corrections to allow for the presence of the train are required. In TWINS, 2D BE calculations have been used to allow for this and to update the vertical directivity of the rail. For ATPA and PBA, in situations where it is not possible to measure transfer functions with the train present, corrections can be applied, either from BE calculations or from previous comparisons of results with and without the train.

Although the results shown have been mainly limited to lower train speeds, it may be noted that the relative source contributions within any one-third octave frequency band obtained from the TWINS or PBA methods are independent of train speed, while those from the ATPA method are similar. However, the results at higher speeds were contaminated by the contribution of other sources at frequencies below 1 kHz, even though the rolling noise was dominant in the overall A-weighted level.

## Statements and Declarations

The authors have no financial or non-financial interests that are directly or indirectly related to the work submitted for publication.


## Acknowledgements

This work has been supported by the TRANSIT project (funded by EU Horizon 2020 and the Europe's Rail Joint Undertaking under grant agreement 881771). The contents of this paper only reflect the authors' views; the Europe's Rail Joint Undertaking is not responsible for any use that may be made of the information contained in the paper. The field tests have been carried out in collaboration with the FINE-2 project which provided the trains and track access. Published data is available from the University of Southampton repository at https://doi.org/10.5258/SOTON/D3244.


## References


1. Commission Regulation (EU) No 1304/2014 of 26 November 2014 on the technical specification for interoperability relating to the subsystem 'rolling stock — noise' amending Decision 2008/232/EC and repealing Decision 2011/229/EU
2. International Organization for Standardization (2013) Acoustics—Railway applications—Measurements of noise emitted by railbound vehicles, ISO 3095:2013, Geneva
3. Janssens MHA, Dittrich MG, de Beer FG, et al (2006) Railway noise measurement method for pass-by noise, total effective roughness, transfer functions and track spatial decay. J Sound Vib 293(3–5):1007–1028
4. European Committee for Standardization (2016) Railway applications – Acoustics – Measurement method for combined roughness, track decay rates and transfer functions, CEN/TR 16891, Brussels
5. H.W. Jansen, M.G. Dittrich, G. Squicciarini et al (2014) Source separation and transposition techniques, ACOUTRAIN report, ACT-T2_4-TNO-023-02
6. H.W. Jansen, M.G. Dittrich, G. Squicciarini et al (2013) Transposition of noise type test data for tracks and vehicles. In: J.C.O. Nielsen, et al. (Eds) Proceedings of 11th International Workshop on Railway Noise, Uddevalla, pp 213–220
7. P.J. Remington (1987) Wheel/rail rolling noise, II: Validation of the theory. Journal of the Acoustical Society of America 81(6): 1824–1832
8. Thompson DJ (1988) Predictions of acoustic radiation from vibrating wheels and rails. J Sound Vib 120(2):275–280

9. D.J. Thompson, B. Hemsworth, N. Vincent (1996) Experimental validation of the TWINS prediction program for rolling noise, part 1: description of the model and method. Journal of Sound and Vibration 193(1): 123–135
10. D.J. Thompson, P. Fodiman, H. Mahé (1996) Experimental validation of the TWINS prediction program for rolling noise, part 2: results. Journal of Sound and Vibration 193(1):137–147.
11. B. Barsikow, W.F. King III, E. Pfizenmaier (1987) Wheel/rail noise generated by a high-speed train investigated by a line array of microphones. Journal of Sound and Vibration 118(1):99–122.
12. B. Barsikow (1996) Experiences with various configurations of microphone arrays used to locate sound sources on railway trains operated by the DB AG. Journal of Sound and Vibration 193(1):283–293
13. G. Hölzl (1996) Low noise goods wagons. Journal of Sound and Vibration 193(1):359–366
14. J.D. van der Toorn, H. Hendricks, T.C. van den Dool (1996) Measuring TGV source strength with Syntacan. Journal of Sound and Vibration 193(1):113–121
15. Dittrich MG, Janssens MHA (2000) Improved measurement methods for railway rolling noise. J Sound Vib 231(3):595–609
16. Brühl S, Röder A (2000) Acoustic noise source modelling based on microphone array measurements. J Sound Vib 231(3):611–617
17. A. Nordborg, A. Martens, J. Wedemann et al (2001) Wheel/rail noise separation with microphone array. In: Proceedings of Inter Noise 2001, Hague
18. Kitagawa T, Thompson DJ (2006) Comparison of wheel/rail noise radiation on Japanese railways using the TWINS model and microphone array measurements. J Sound Vib 293(3–5):496–509
19. T. Kitagawa, D.J. Thompson (2010) The horizontal directivity of noise radiated by a rail and implications for the use of microphone arrays. Journal of Sound and Vibration 329(2): 202–220
20. J. Zhang, G. Squicciarini, D.J. Thompson (2019) Implications of the directivity of railway noise sources for their quantification using conventional beamforming. Journal of Sound and Vibration 459:114841
21. Thompson DJ, Jones CJC, Turner N (2003) Investigation into the validity of two-dimensional models for sound radiation from waves in rails. J Acoust Soc Am 113(4):1965–1974
22. D.J. Thompson (2024) Railway noise and vibration: mechanisms, modelling and means of control, Second edition. Elsevier, London,
23. B. Faure, O. Chiello, M.A. Pallas et al (2015) Characterisation of the acoustic field radiated by a rail with a microphone array: the SWEAM method. Journal of Sound and Vibration 346:165–190

24. E. Zea, E. Fernandez-Grande, I. Lopez Arteaga (2020) Separation of rail and wheel contributions to pass-by noise with sparse regularization methods. Journal of Sound and Vibration 487:115627
25. M.H.A. Janssens, J.W. Verheij, D.J. Thompson (1999) The use of an equivalent forces method for quantifying structural sound transmission in ships. Journal of Sound and Vibration 226(2):305–328
26. D.J. Thompson, G. Squicciarini, J. Wändell et al (2017) Roll2Rail Deliverable D7.4—Assessment and validation of source separation methods
27. Thompson D, Squicciarini G, Zhang J et al (2018) Assessment of measurement-based methods for separating wheel and track contributions to railway rolling noise. Appl Acoust 140:48–62
28. F.X. Magrans (1981) Method of measuring transmission paths. Journal of Sound and Vibration 74(3):321–330
29. F. Létourneaux (2003) MISO: A measurement method to separate noise emission of railway vehicles and tracks, STAIRRS Report - D11 Part 5
30. Thompson D, Zhao D, Cierco E, et al (2024) Improved methods for the separation of track and wheel noise components during a train pass-by. Lecture Notes in Mechanical Engineering. Springer, Singapore
31. C.J.C. Jones, D.J. Thompson (2003) Extended validation of a theoretical model for railway rolling noise using novel wheel and track designs. Journal of Sound and Vibration 267(3):509–522.
32. X. Zhang, D. Thompson, H. Jeong et al (2020) Measurements of the high frequency dynamic stiffness of railway ballast and subgrade. Journal of Sound and Vibration 468:115081
33. X. Zhang, G. Squicciarini, D.J. Thompson (2016) Sound radiation of a railway rail in close proximity to the ground. Journal of Sound and Vibration 326:111–124
34. X. Zhang, D.J. Thompson, G. Squicciarini (2016) Sound radiation from railway sleepers. Journal of Sound and Vibration 369:178–194
35. X. Zhang, D.J. Thompson, E. Quaranta (2019) An engineering model for the prediction of the sound radiation from a railway track. Journal of Sound and Vibration 461:114921
36. D. Thompson, D. Zhao, E. Ntotsios et al (2024) The influence of reflections from the train body and the ground on the sound radiation from a railway rail, Railway Sciences 3(1): 1–17
37. F.J. Fahy (1995) The vibro-acoustic reciprocity principle and applications to noise control. Acustica 81(6):544–558
38. D.J. Thompson, D. Zhao, E. Cierco (2023) Track and vehicle separation and transposition techniques: conclusions, recommendations and validation test results, TRANSIT Deliverable D3.3